REPORT DOCUMENTATION PAGE

Form Approved
OMB No. 0704-0188

1. REPORT DATE *(DD-MM-YYYY)*	2. REPORT TYPE	3. DATES COVERED *(From - To)*
12/10/2018	Final Technical	01/01/2016 - 09/30/2018

4. TITLE AND SUBTITLE

Distributed spatiotemporal dynamics of synthetic gene circuits

5a. CONTRACT NUMBER

5b. GRANT NUMBER
N00014-16-1-2093

5c. PROGRAM ELEMENT NUMBER

6. AUTHOR(S)
Lev Tsimring

5d. PROJECT NUMBER

5e. TASK NUMBER

5f. WORK UNIT NUMBER

7. PERFORMING ORGANIZATION NAME(S) AND ADDRESS(ES)
University of California, San Diego, BioCircuits Institute
9500 Gilman Drive, Mail Code 0328
La Jolla, CA 92093-0328

8. PERFORMING ORGANIZATION REPORT NUMBER

9. SPONSORING/MONITORING AGENCY NAME(S) AND ADDRESS(ES)
Office of Naval Research REG Office San Diego
140 Sylvester Road, Bldg. 140 Room 218
San Diego, CA 92106

10. SPONSOR/MONITOR'S ACRONYM(S)
ONR

11. SPONSORING/MONITORING AGENCY REPORT NUMBER
N66018

12. DISTRIBUTION AVAILABILITY STATEMENT
Approved for public release; distribution unlimited.

13. SUPPLEMENTARY NOTES

14. ABSTRACT

In this project we developed a multi-scale computational approach for analysis of multi-cellular processes in large bacterial populations and design of distributed synthetic gene circuits. This approach integrates discrete agent simulations of single cells with PDE modeling of large-scale dynamics. We applied this framework to computational modeling of spatiotemporal dynamics of growing bacterial biofilms and the dynamics of multi-strain bacterial populations.

15. SUBJECT TERMS
bacterial populations, multi-cellular dynamics, multi-scale modeling, pattern formation, gene regulatory networks

16. SECURITY CLASSIFICATION OF:			17. LIMITATION OF ABSTRACT	18. NUMBER OF PAGES	19a. NAME OF RESPONSIBLE PERSON
a. REPORT	b. ABSTRACT	c. THIS PAGE			Lev Tsimring
U	U	U	SAR	13	19b. TELEPONE NUMBER *(Include area code)* (858) 534-0816

Distributed spatiotemporal dynamics of synthetic gene circuits

University of California, San Diego

PI: Lev Tsimring
Research Scientist
BioCircuits Institute
9500 Gilman Drive
Mail Code 0328
University of California, San Diego
La Jolla, CA 92093-0328
Tel: 1 (858) 534-0816
FAX: 1 (858) 534 1892
email: ltsimring@ucsd.edu

Agreement No. N00014-16-1-2093
Final Technical Report

1 Introduction

The difficulties in quantitative studies of biological systems stem not only from the complexity of underlying dynamical networks but from the inherent multi-scale nature of emergent biological phenomena and considerable variability in the responses of even genetically identical cells. The structure of multi-cellular communities, tiossues and whole organisms depends crucially on the properties of individual cells and sub-cellular phenomena, where stochasticity of underlying biochemical reactions and cell-cell variability plays an important role. That was our primary motivation in this work where we proposed to implement a multi-scale approach to the description of microbial communities.

To achieve this goal required a multi-disciplinary approach integrating computational modeling and molecular biology, along with the development of novel experimental assays utilizing microscopy and microfabrication techniques for testing and validating the computational models. We proposed to combine microfluidic technology with computational modeling to develop a platform that integrates the dissection, culturing, monitoring and quantification of natural ecosystems and the construction of functional synthetic communities.

Our work on this grant followed two main directions outlined in the subsequent sections.

2 Computational modeling of spatiotemporal dynamics of bacterial biofilms

In this course of working on grant, we developed a mathematical framework that connects single-cell dynamics with population-level dynamics in microbial consortia. It spans multiple scales by simulating large-scale population dynamics using deterministic partial differential equations and agent-based discrete models to directly model stochastic single-cell dynamics.

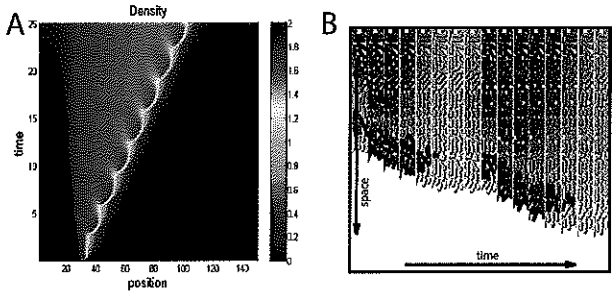

Figure 1: *(A) Space-time plot of the biofilm density from the coarse-grained PDE model. (B) Kymograph of the oscillating front motion from the agent-based model. Each vertical column is a cutout from snapshots separated by 15 min. Red color indicates the concentration of ammonium, and blue color denotes the growing cells.*

At first, we applied this approach to modeling bacterial dynamics in and around a growing biofilm in collaboration with Prof. Gürol Süel (UCSD). In his recent paper they discovered regular oscillatory patterns in biofilm growth which were attributed to an intricate separation of labor during bacterial metabolism. We developed a multi-scape approach to quantitatively describe this process. Specifically, we constructed a continuum model consisting of three reaction-diffusion equations for the glutamate and ammonium concentrations and the cell density. Our simulations with this model indeed showed robust oscillations of the biofilm expansion rate (Fig. 1A) in agreement with recent experimental observations [1].

Concurrently, we developed a microscopic model for single-cell dynamics within the biofilm. It is based on the agent-based model for bacterial growth and ordering that we formulated earlier [2–4] to describe mechanical forces between bacteria in dense bacterial

colonies. In the present implementation, we added to the model of individual cells intracellular biochemical reactions comprising bacterial metabolism (Fig. 1B). Each cell in the population is modeled as a spherocylinder that can grow along its axis and divide once the conditions for division are met. Each cell is endowed with a set of ordinary differential equations describing metabolic reactions and biomass growth, which uses as input time-dependent parameters of the local extracellular concentrations of ammonium and glutamate. In turn, each cell serves as a localized source and/or a sink of the glutamate and ammonium that diffuses through the cell membrane and throughout the integration domain. Some results of our simulations of this model are shown (Fig. 1). Panel A shows a snapshot form a typical simulation depicting the cells within a narrow channel in the presence of externally supplied glutamate. Simulation shows that only cells localized near the front, where glutamate is still present, can grow (blue-colored cells). This growth of peripheral cells is supported by ammonium produced by interior cells (red-colored cells). Kymograph in Panel B shows the time-periodic advancement of the cell front accompanied by periodic modulation in ammonium synthesis in the simulations of the agent-based model.

In the follow-up study we applied the same framework to the analysis and simulations of the interplay between bacterial growth and motility dynamics. A recently discovered signaling mechanism [5], based on ion channel mediated electrical cell-to-cell signaling, has been shown to facilitate efficient long-range communication within a biofilm community. Specifically, it was demonstrated that cells within *B. subtilis* biofilms can actively relay extracellular potassium signals, producing electrical waves that propagate through the biofilm and coordinate metabolic states, thereby increasing collective fitness. In collaboration with Süel group we investigated whether electrical signals generated within the biofilm can influence the behavior of distant motile bacteria that share the same aqueous environment. In particular, we hypothesized that electrical signals could direct bacterial motility through altering the membrane potential. Such long-range signaling could provide a mechanism for recruiting new members to the community.

We used our hybrid agent-based approach by combining single-cell modeling of intracellular dynamics and PDE model for the extracellular potassium field. We utilized an electrophysiological model based on the mathematical framework developed by Hodgkin and Huxley (1952) to predict changes in membrane potential in response to extracellular potassium [5]. This model was constrained by the measurement of membrane potential dynamics observed in distant stationary cells. We integrated this electrophysiological model with an agent-based physical model [2, 3] to simulate the motility of individual cells (see Fig. 2A for details of the agent-based model). In brief, cells were modeled as soft spherocylinders that moved according to Newtons law under the forces and torques caused by their own motility and contacts with other cells. In a departure from earlier models [2,3,5], each cell was endowed with a set of ordinary differential equations coupling its electrophysiological state with its motility (Fig. 2A). Using this model, we computed how a change in extracellular potassium altered the cells membrane potential and how this in turn affected the tumbling probability of each motile cell (Fig. 2A). Furthermore, the simulations contained non-motile biofilm cells that were assumed to alternate between acting as a source or sink of potassium (peak and trough electrical activity respectively) (Fig. 2B, cyan and black cells, respectively). The spread of extracellular potassium through the medium was described by the standard diffusion equation. Consistent with experimental results, simulations showed periodic attraction of distant motile cells

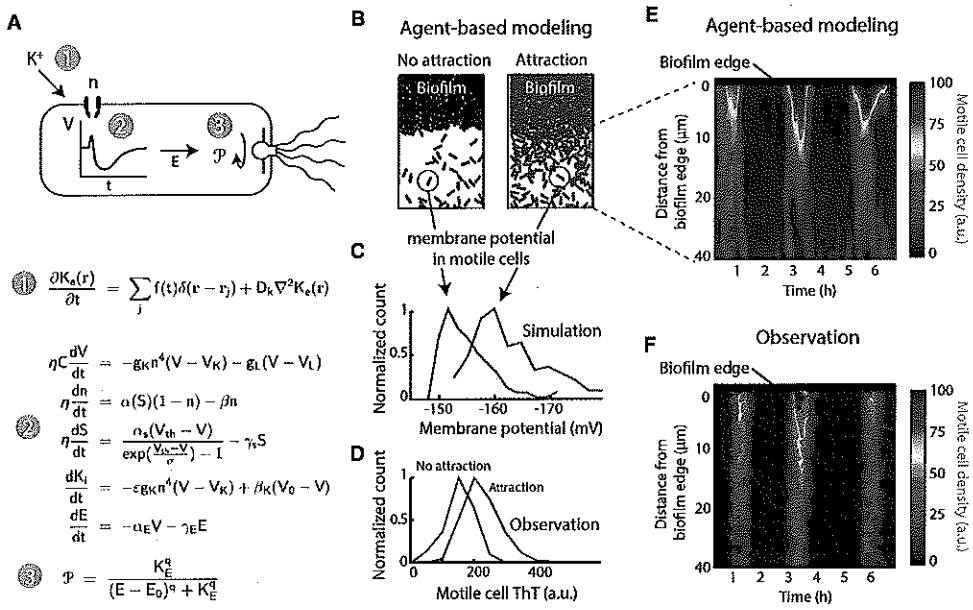

Figure 2: *Agent-Based Modeling of Motile Cell Attraction Driven by Electrical Signaling from Biofilms (A) Top: schematic illustrating how extracellular potassium alters motility by changing the membrane potential. Step 1: extracellular potassium depolarizes the cell. Step 2: depolarization prompts adaptation by the cell leading to hyperpolarization. Step 3: hyperpolarization increases the proton motive force, thus directing motility by altering the tumbling frequency of the cell. Bottom: the computational model encompassing: (1) spatiotemporal reaction-diffusion model for the extracellular potassium Ke dynamics; (2) intracellular electrophysiological model for the cell membrane potential V, ion channel state n, metabolic stress S, intracellular potassium Ki, and energy needed to drive the flagellar motor E; and (3) discrete biomechanical model for individual cell motion influenced by their internal motility and interaction with other cells. The motility of individual cells is affected by the internal cellular state E via the change of the probability of tumbling P. (B) Two snapshots of the combined agent-based simulation show increased density of motile (red) cells near the biofilm during the peak of the attraction phase to the biofilm. Biofilm cells are colored according to their membrane potential during each time point, where cyan coloring indicates more negative membrane potential relative to black coloring. (C) Distributions of membrane potential in motile cells from the computational model indicate that motile cell membrane potential is more negative during the peak of the attraction phase to the biofilm. (D) Experimental data confirm the modeling prediction that the distribution of motile cell membrane potential (ThT, a.u.) is more negative during attraction to the biofilm compared to the non-attraction phase. (E) Plot of motile cell density in the first 40 mm away from the biofilm edge over time, obtained from agent-based modeling simulations of motile cell attraction. The region closest to the biofilm edge is located at the top of the plots for both (E) and (F) and distance from the biofilm edge increases moving downward. (F) Experimental data show similar motile cell density dynamics in the first 40 mm away from the biofilm edge.*

to an electrically oscillating biofilm (Fig. 2B). These modeling results demonstrate that an oscillating source (biofilm) of extracellular potassium can periodically attract motile cells by changing their membrane potential.

Our model was predominantly informed by measurements in stationary cells, providing the opportunity to independently validate modeling predictions through additional motile cell measurements. In particular, we tested the modeling prediction that motile cells moving along a spatial potassium gradient are expected to have a similar membrane potential profile as stationary cells responding to temporal changes of potassium (Fig. 2C). In other words, motile cells during peak biofilm electrical activity should on average have a more negative membrane potential. To test this prediction, we measured the

distribution of membrane potential in motile cells specifically at the attraction (peak) and non-attraction (trough) phases of the electrical oscillations in the biofilm. As predicted by our model, we find that motile cells have on average a more negative membrane potential in the attraction phase (Figure 2D). These data show that similar to stationary cells, the membrane potential of motile cells also depends on the electrical activity of the biofilm. In addition, we find that the motile cell density profile as a function of time and distance from the biofilm is consistent with modeling predictions (Figures 2E and 2F). Together, these results further validate the mathematical model and allow us to establish a coherent framework to interpret experimental observations.

hese results was published in the journal "Cell" [6].

3 Pattern formation in the synthetic two-strain bacterial system

In natural habitats, microorganisms often form multi-strain communities with intricate social organization and complex spatial structure [7]. The repertoire of interactions among microorganisms is very diverse and includes cooperation [8, 9], competition for common resources [10, 11], and predation [12–14]. One major question drawing significant interest is how different microbial species may stably coexist within a common environment in the presence of competition and predation [10, 15]. In this grant, we studied this question theoretically, focusing on one ubiquitous mechanism of bacterial predation: contact-dependent killing of neighboring cells by direct injection of lethal toxins via the type VI secretion system (T6SS) [16–22]. The T6SS has been found in many genera of bacteria, including *Vibrio*, *Pseudomonas*, and *Acinetobacter*.

We developed a computational model that describes pattern formation in a mixture of two bacterial strains, stain 1 (*E. coli*) and strain 2 (*A. baylyi*), in which strain 1 has growth advantage, but strain 2 is capable of lysing strain 1 on direct contact (T6 secretion system). Furthermore, strain 1 produces a fast- diffusing quorum-sensing molecule AHL that inhibits growth of stain 1. The coarse-grained model for the population dynamics includes two equations for the cell densities n_1, n_2 for both strains and the equation for the fast-diffusing quorum-sensing molecule AHL, A:

$$\partial_t n_1 = \gamma_1 f(A) n_1 \left[1 - \frac{n_1 + n_2}{n_0}\right] - \delta n_1 - \kappa n_1 n_2 + D_n \nabla^2 n_1 \quad (1)$$

$$\partial_t n_2 = \gamma_2 n_2 \left[1 - \frac{n_1 + n_2}{n_0}\right] - \delta n_2 + D_n \nabla^2 n_2 \quad (2)$$

$$\partial_t A = \gamma_A n_1 - \delta_A A + D_A \nabla^2 A \quad (3)$$

Here function $f(A) = 1/(1 + A)$ describes the inhibiting effect of the quorum-sensing molecules AHL on the growth of strain 1. If in the absence of AHL strain 1 grows faster than strain 2 ($\gamma_1 > \gamma_2$), for a certain killing efficiency κ this system exhibits bistability: both "pure" solutions $n_1 = 0, n_2 = n_2^*$ and $n_1 = n_1^*, n_2 = 0$ are linearly stable. The front between these two states can propagate in either direction depending on parameters. However the front propagation towards strain 2 would eventually saturate because of inhibiting action of the quorum sensing molecule, thus forming a stable interface. For smaller difference in growth rates of n_1 and n_2, the interface between the two populations will propagate towards n_1, thereby reducing the fraction of n_1 in a mixture. That in turn will reduce the amount of AHL, accelerate growth of n_1, and stabilize the fronts. Two-dimensional sim-

ulations of model (1) show that this system forms a regular pattern of *E. coli* "droplets" surrounded by *A. baylyi* . In different parameter regions, an inverse pattern of *A. baylyi* droplets surrounded by *E. coli*, can be formed (see Fig. 3).

We performed a full bifurcation analysis of this system in the spatially-homogeneous case when n_1, n_2 and A are only functions of time. In a certain range of parameters the system exhibits bistability: either of the two strains may stably dominate depending on the initial ratio of concentrations. In a spatially-nonuniform case, the system may phase-separate: the region with pure n_1 and pure n_2 will be separated by the fronts, or interfaces. These interfaces would move in either direction depending on the system parameters, but eventually will stabilize because the inhibitor field A plays the role of stabilizer: if the front initially propagates towards n_2 (when n_1 is more stable), the concentration of A will grow, and it will slow down the growth of n_1 and hence slow down the front propagation. In the opposite case, when the n_2 region initially expands, the concentration of A will decrease because of shrinkage of $n1$, and the growth of n_1 will accelerate, and the pattern will stabilize again. We demonstrated theoretically that the islands of n_1 of a certain characteristic size will emerge. These islands, or spots, in two dimensions will slowly form a quasi-regular pattern because of exponentially weak interaction among them (see Fig. 3).

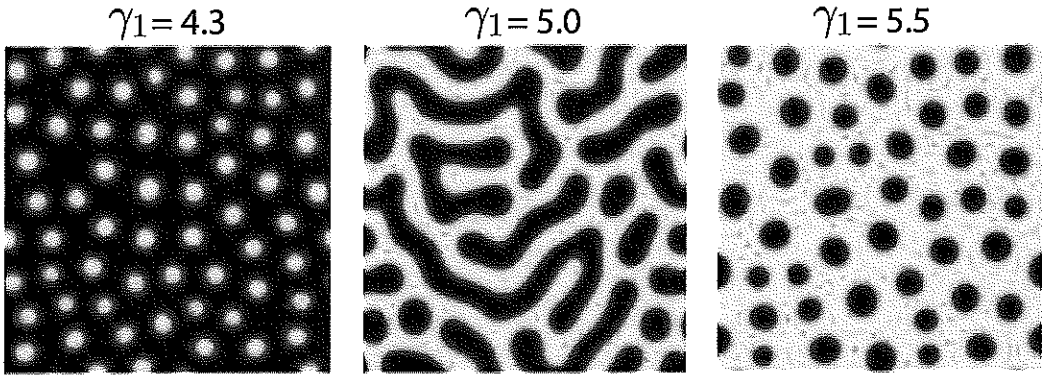

Figure 3: *(A) Formation of stable cellular patterns in 2-D deterministic model for different* γ_1*. Other model parameters:* $\delta = 0.01$, $\kappa = 0.03$, $\gamma_A = 0.04$, $\delta_A = 0.02$.

We also developed a lattice-based discrete-element model that mimics stochastic population dynamics of two bacterial strains. We assume that each node of a square lattice may contain an integer number of T6SS-sensitive and T6SS-active cells, n_1 and n_2, respectively. At every time step, each cell can divide with a probability that is equal to its growth rate (γ_1 or γ_2, respectively) thereby increasing the occupancy number of the corresponding cell type in that lattice site by one. We assume that each lattice site can only accommodate no more than n_0 cells, and so once the total number of cells $n_1 + n_2$ at a certain lattice site reaches n_0, cell division at that site is suspended. To model the short-range cell motility, we allow cells to hop to any of four neighboring lattice sites with equal rates D_n, if that neighboring site has a vacancy. A cell can also spontaneously die with probability δ, thus reducing the number of cells of its type in its lattice site by one. Finally, a type-2 cells can kill type-1 cells with probability κ if they occupy the same site, thus reducing the occupancy number n_1 by one. All these processes are simulated as independent Markovian events. We also introduce a real-valued inhibitor field A that is defined on the same lattice.

It is produced at each lattice site in proportion of the corresponding n_1 value, degraded with rate δ_A and diffused with the diffusion constant D_A. The spatio-temporal evolution of A was simulated deterministically using the first-order split-step pseudo-spectral method. We employed a 512×512 lattice with periodic boundary conditions.

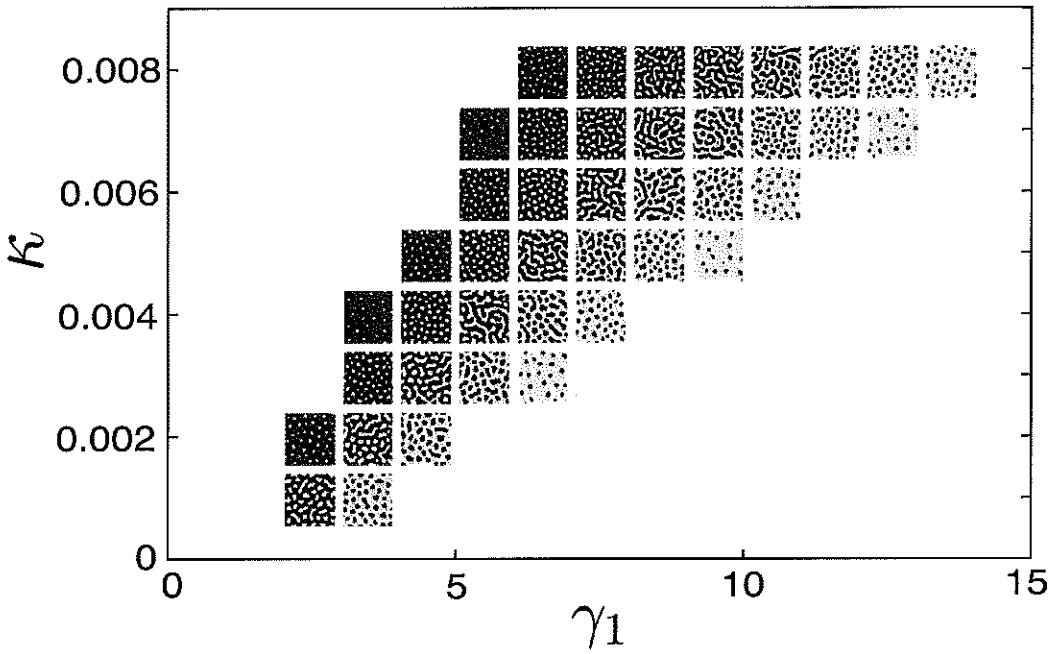

Figure 4: *Typical patterns emerging from random initial conditions in stochastic simulations for different values of parameters κ and γ_1. Other parameters are: $\gamma_2 = 1, n_0 = 10, \delta = 0.01, \delta_A = 0.02, \gamma_A = 0.004, D_n = 0.1, D_A = 12.5$. System size is 256×256. Because the number of cells must be integers in stochastic simulations, we use unscaled parameters here.*

We ran a series of discrete stochastic simulations at range of values of γ_1 and κ. Again, the initial condition for these simulations was a sparse random mixture of n_1 and n_2 cells. In agreement with the continuum theory, in the bulk of the region where the existence of stable patterns was expected, the patterns indeed spontaneously emerged, see Fig. 4. As seen from this figure, depending on the relative growth advantage of type-1 strain and the killing efficiency by type-2 strain, the patterns change their structure: for smaller γ_1/γ_2 or larger κ, they appear as isolated islands of n_1 surrounded by n_2. For large growth advantage of type-1 strain or small κ, the patterns are reversed: the islands of n_2 are surrounded by the sea of n_1. In the intermediate range, we found more symmetric labyrinthine patterns.

We also tested our theoretical and computational findings in experiment with a mixture of T6SS-active and T6SS-sensitive bacteria . We used Gram-negative bacteria *A. baylyi* [23,24] which is known to be T6SS-active, and the lab strain of *E. coli* that is T6SS-sensitive. The *E.coli* bacteria were transformed with a plasmid containing constitutively expressed mTFP (green), and *A. baylyi* was transformed with a plasmid containing constitutively expressed mCherry gene (red). The growth rate of *E. coli* and *A. baylyi* in liquid culture measured in a plate reader were 0.0327 ± 0.0001 min^{-1} (mean $\pm$ SE, $n = 3$) and 0.0165 ± 0.0009 min^{-1} (mean $\pm$ SE, $n = 3$) respectively. We inoculated dilute mixtures of *E. coli* and *A. baylyi* with different initial concentrations on a surface of 1.5% agar in a Petri dish and grew them at 37 °C under a fluorescent microscope. The fluorescence became

visible after about 24h of cell growth and revealed small-scale structural inhomogeneities that gradually became more and more pronounced. About 3 days after inoculation, the patterns typically stabilized [Fig. 5(a)]. We analyzed fluorescent images and computed the distributions of sizes could be calculated [Fig. 5(b)]. We found that the distribution had a peak at about $120\mu m^2$, and the position of this peak was quite robust with respect to the relative initial dilutions. However, we noticed that a more uniform dilution ratio 1:5 produces a slightly tighter distribution of spot sizes than a mixture with less concentration of *A. baylyi* .

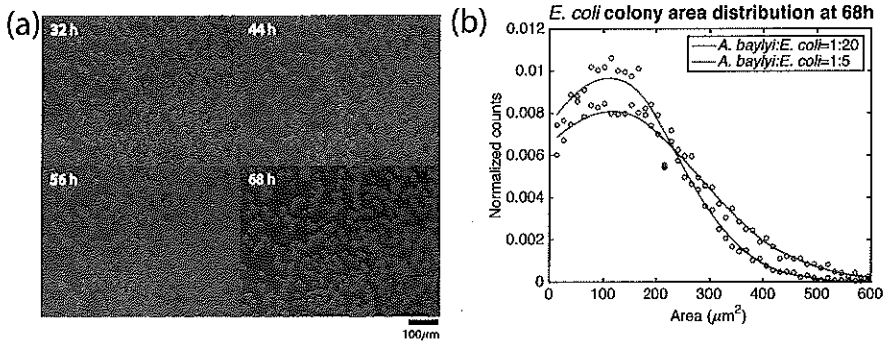

Figure 5: *Pattern formation in mixture of* E. coli *and* A. baylyi *in experiments. (a) Time-lapse images of pattern dynamics in mix of* E. coli *and T6SS*$^+$ A. baylyi *with initial density ratio 5:1.* A. baylyi *cells are labelled by mCherry and* E. coli *cells are labelled by mTFP. (b) Distribution of* E. coli *colony sizes after 68 hours of the inoculation of the mix of* E. coli *and T6SS*$^+$ A. baylyi.

These results were published in the *Biophysical Journal* [25].

We also studied the emergence of complex structures in a biofilm grown from a small drop of a mixtures of motile and non-motile strains of bacteria on a semi-solid agar surface theoretically and experimentally. Specifically, we again studied the interactions between *A. baylyi* , a gram-negative bacterium that easily moves on semi-solid surfaces using twitching motility, and an *E. coli* strain that is almost non-motile on semi-solid agar. We found that when these two strains are mixed together and inoculated on agar surface, a growing biofilm develops a flower-like structure that is entirely absent when either species is grown by itself. By observing the spatiotemporal dynamics of the growing biofilm using time-lapse fluorescent microscopy, we found that non-motile *E. coli* are pushed outward by motile *A. baylyi* and concentrate at the periphery of the colony. The colony initially has a nearly circular shape in which a filled circle of *A. baylyi* is surrounded by a band of *E. coli* . As the colony grows, the outer band visibly becomes unstable, the undulations grow to form "cusps" in which the concentration of *E. coli* is much higher than elsewhere. As these cusps travel forward pushed by growing *A. baylyi* , they leave behind trails of *E. coli* that looks like branches. These branches gradually merge together, while new cusps percolate at the interface and give rise to new branches. As a result, an intricate flower-like pattern emerges in the interior of the colony (see Fig. 6). To shed light on the mechanism behind such intricate pattern formation, we tested whether specific modes of cell-cell communication played a role there or they were a result of more generic interaction of strains with diverging motility properties. Wild-type *A. baylyi* possesses a well-characterized T6 secretion system that enables them to kill other bacteria (including *E. coli*) on direct contact. However, experiments with *A. baylyi* mutants

lacking T6SS showed that the flower-like pattern formation did not rely on this mechanism. On the other hand, reducing motility of *A. baylyi* by another genetic manipulation eliminated the patters entirely.

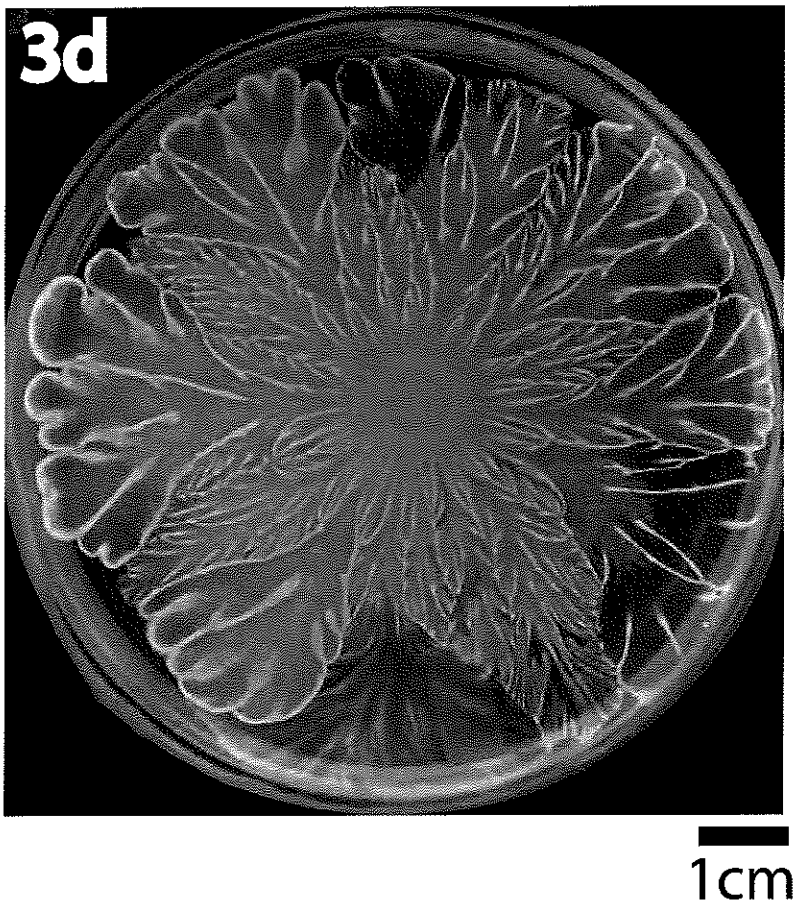

Figure 6: *Flower-like patterns in a mixture of* E. coli *and* A. baylyi *three days after inoculation.*

To further confirm that differences in cell motility are sufficient to explain the pattern formation, we performed theoretical and computational analysis of two conceptually different models describing the mechanical interaction of two strains. The first model is only concerned with the dynamics of the colony interface that it describes as a one-dimensional curve that moves under the combined action of interior pressure and friction that is modulated by inhomogeneous stretching of the interface. This model naturally gives rise to the interface instability that develops highly localized cusps and, presumably, can generate branching and flower-like structures in its wake (see Fig. 7).

We also developed a more realistic 2D model of two growing and mechanically interacting strains that is similar in spirit to phase-field models of cell morphodynamics [26, 27]. This model exhibits the same type of interface instability and produces flower-like patterns in the interior of the growing colony (see Fig. 8). Our findings suggest that the interplay between an outward pressure force and friction within microbial communities

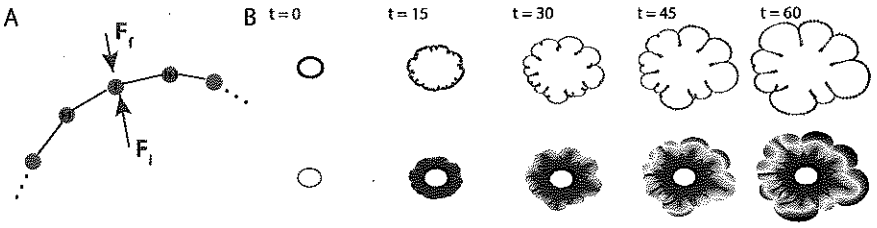

Figure 7: *Discrete interface model. (A) A sketch of the model. F_0 is the active force driven by* A. baylyi . *F_f is the friction force provided by* E. coli *which is proportional to the nodes density. (B) Evolution of the interface. Top: interface dynamics; Bottom: traces of the nodes on the interface.*

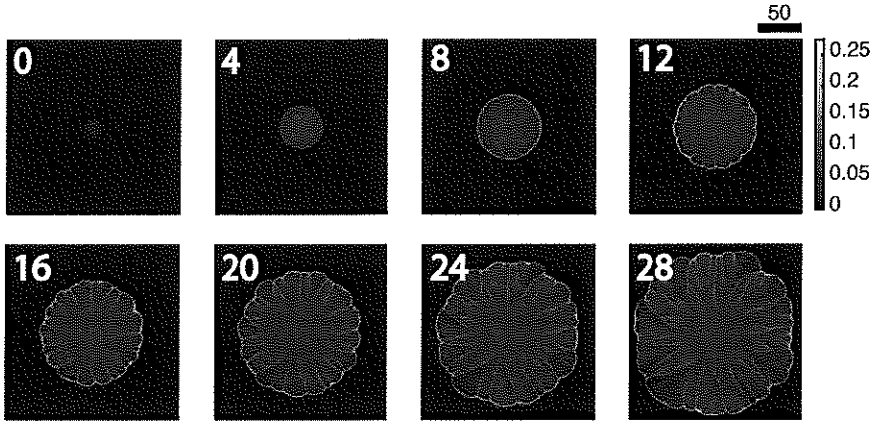

Figure 8: *Phase-field model simulations of the two-strain colony growth*

can lead to complex heterogeneous biofilm structures.

Our findings highlight the importance of mechanical interactions in shaping the spatial structure of multi-strain biofilms. The manuscript describing this study will soon be submitted for publication.

References

[1] Jintao Liu, Arthur Prindle, Jacqueline Humphries, Marçal Gabalda-Sagarra, Munehiro Asally, D Lee Dong-yeon, San Ly, Jordi Garcia-Ojalvo, and Gürol M Süel. Metabolic co-dependence gives rise to collective oscillations within biofilms. *Nature*, 523(7562):550–554, 2015.

[2] Dmitri Volfson, Scott Cookson, Jeff Hasty, and Lev S Tsimring. Biomechanical ordering of dense cell populations. *Proceedings of the National Academy of Sciences*, 105(40):15346–15351, 2008.

[3] William Mather, Octavio Mondragón-Palomino, Tal Danino, Jeff Hasty, and Lev S Tsimring. Streaming instability in growing cell populations. *Physical review letters*, 104(20):208101, 2010.

[4] Denis Boyer, William Mather, Octavio Mondragón-Palomino, Sirio Orozco-Fuentes, Tal Danino, Jeff Hasty, and Lev S Tsimring. Buckling instability in ordered bacterial colonies. *Physical biology*, 8(2):026008, 2011.

[5] Arthur Prindle, Jintao Liu, Munehiro Asally, San Ly, Jordi Garcia-Ojalvo, and Gürol M Süel. Ion channels enable electrical communication in bacterial communities. *Nature*, 527(7576):59–63, 2015.

[6] Jacqueline Humphries, Liyang Xiong, Jintao Liu, Arthur Prindle, Fang Yuan, Heidi A Arjes, Lev Tsimring, and Gürol M Süel. Species-independent attraction to biofilms through electrical signaling. *Cell*, 168(1):200–209, 2017.

[7] Reed M Stubbendieck, Carol Vargas-Bautista, and Paul D Straight. Bacterial communities: interactions to scale. *Frontiers in microbiology*, 7:1234, 2016.

[8] Ashleigh S Griffin, Stuart A West, and Angus Buckling. Cooperation and competition in pathogenic bacteria. *Nature*, 430(7003):1024–1027, 2004.

[9] Joao B Xavier, Wook Kim, and Kevin R Foster. A molecular mechanism that stabilizes cooperative secretions in pseudomonas aeruginosa. *Molecular Microbiology*, 79(1):166–179, 2011.

[10] Michael E Hibbing, Clay Fuqua, Matthew R Parsek, and S Brook Peterson. Bacterial competition: surviving and thriving in the microbial jungle. *Nature Reviews Microbiology*, 8(1):15–25, 2010.

[11] Olaya Rendueles and Jean-Marc Ghigo. Mechanisms of competition in biofilm communities. *Microbiology Spectrum*, 3(3):MB–0009–2014, 2015.

[12] H Stolp and MP Starr. Bdellovibrio bacteriovorus gen. et sp. n., a predatory, ectoparasitic, and bacteriolytic microorganism. *Antonie Van Leeuwenhoek*, 29(1):217–248, 1963.

[13] Susan C Straley and SF Conti. Chemotaxis by bdellovibrio bacteriovorus toward prey. *Journal of Bacteriology*, 132(2):628–640, 1977.

[14] Klaus Jürgens and Carsten Matz. Predation as a shaping force for the phenotypic and genotypic composition of planktonic bacteria. *Antonie van Leeuwenhoek*, 81(1-4):413–434, 2002.

[15] Katharine Z Coyte, Jonas Schluter, and Kevin R Foster. The ecology of the microbiome: networks, competition, and stability. *Science*, 350(6261):663–666, 2015.

[16] Stefan Pukatzki, Amy T Ma, Derek Sturtevant, Bryan Krastins, David Sarracino, William C Nelson, John F Heidelberg, and John J Mekalanos. Identification of a conserved bacterial protein secretion system in Vibrio cholerae using the Dictyostelium host model system. *Proceedings of the National Academy of Sciences, USA*, 103(5):1528–1533, 2006.

[17] Petr G Leiman, Marek Basler, Udupi A Ramagopal, Jeffrey B Bonanno, J Michael Sauder, Stefan Pukatzki, Stephen K Burley, Steven C Almo, and John J Mekalanos. Type VI secretion apparatus and phage tail-associated protein complexes share a

common evolutionary origin. *Proceedings of the National Academy of Sciences, USA*, 106(11):4154–4159, 2009.

[18] M Basler, M Pilhofer, GP Henderson, GJ Jensen, and JJ Mekalanos. Type VI secretion requires a dynamic contractile phage tail-like structure. *Nature*, 483(7388):182–186, 2012.

[19] Lisa G Pell, Voula Kanelis, Logan W Donaldson, P Lynne Howell, and Alan R Davidson. The phage λ major tail protein structure reveals a common evolution for long-tailed phages and the type VI bacterial secretion system. *Proceedings of the National Academy of Sciences, USA*, 106(11):4160–4165, 2009.

[20] Véronique de Berardinis, David Vallenet, Vanina Castelli, Marielle Besnard, Agnes Pinet, Corinne Cruaud, Sumitta Samair, Christophe Lechaplais, Gabor Gyapay, Céline Richez, et al. A complete collection of single-gene deletion mutants of acinetobacter baylyi adp1. *Molecular Systems Biology*, 4(1):174, 2008.

[21] Michael D Carruthers, Paul A Nicholson, Erin N Tracy, and Robert S Munson Jr. Acinetobacter baumannii utilizes a type VI secretion system for bacterial competition. *PloS one*, 8(3):e59388, 2013.

[22] M Basler and JJ Mekalanos. Type 6 secretion dynamics within and between bacterial cells. *Science*, 337(6096):815–815, 2012.

[23] Valerie Barbe, David Vallenet, Nuria Fonknechten, Annett Kreimeyer, Sophie Oztas, Laurent Labarre, Stephane Cruveiller, Catherine Robert, Simone Duprat, Patrick Wincker, et al. Unique features revealed by the genome sequence of acinetobacter sp. adp1, a versatile and naturally transformation competent bacterium. *Nucleic Acids Research*, 32(19):5766–5779, 2004.

[24] David Metzgar, Jamie M Bacher, Valérie Pezo, John Reader, Volker Döring, Paul Schimmel, Philippe Marlière, and Valérie de Crécy-Lagard. Acinetobacter sp. adp1: an ideal model organism for genetic analysis and genome engineering. *Nucleic acids research*, 32(19):5780–5790, 2004.

[25] Liyang Xiong, Robert Cooper, and Lev S Tsimring. Coexistence and pattern formation in bacterial mixtures with contact-dependent killing. *Biophysical journal*, 114(7):1741–1750, 2018.

[26] Danying Shao, Wouter-Jan Rappel, and Herbert Levine. Computational model for cell morphodynamics. *Physical review letters*, 105(10):108104, 2010.

[27] Danying Shao, Herbert Levine, and Wouter-Jan Rappel. Coupling actin flow, adhesion, and morphology in a computational cell motility model. *Proceedings of the National Academy of Sciences*, 109(18):6851–6856, 2012.